Nanoscale

Accepted Manuscript

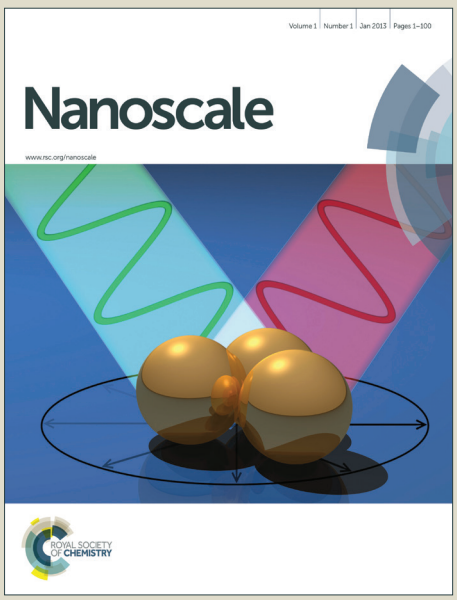

ROYAL SOCIETY OF CHEMISTRY

www.rsc.org/nanoscale

Manuscript for ***Nanoscale*** as ***communication***

Noninvasive label-free nanoplasmonic optical imaging for real-time monitoring of *in-vitro* amyloid fibrogenesis

Sung Sik Lee[1,5], and Luke P. Lee[2,3,4, *]

[1] Department of Biosystems Science and Engineering, ETH Zurich,

CH 4056, Basel, Switzerland

[2] Department of Bioengineering, [c] Biophysics Program,

[3] Department of Electrical Engineering and Computer Science,

[4] University of California Berkeley, CA 94720-1762, Berkeley, United States

[5] Current address: Institute of Biochemistry, ETH Zurich, CH 8093, Zurich, Switzerland

*to whom correspondence should be addressed:

Luke P. Lee

Department of Bioengineering, University of California at Berkeley, 408C Stanley Hall, Berkeley, CA 94720-1762, United States of America

Tel: (510) 642-5855

Fax: (510) 642-5835

E-mail: lplee@berkeley.edu

ABSTRACT

It is important to develop noninvasive label-free detection method to monitor dynamic phenomena in biology and medicine. Here, we utilize nanoplasmonic optical imaging as the noninvasive and label-free method in order to monitor *in-vitro* amyloid fibrogenesis in real-time, which is considered as the primary pathological mechanism of Alzheimer's disease. Using Rayleigh scattering of gold nanoplasmonic probes (GNPs), which have an enhanced scattering optical cross section due to the surface plasmon resonance of GNPs, we accomplished efficient tracking of the random movements of the GNPs in A*β* solution, and quantified the kinetics of the fibrogenesis. We expect this noninvasive and label-free *in-vitro* method can be utilized in monitoring in wide range of other research field as well. As future applications, we can envision long-term monitoring in neuronal cells to elucidate the mechanism of amyloid growth and NIR-based *in-vivo* imaging with nanoplasmonic optical antennas for gene delivery, photonic gene circuits, and monitoring toward the theranostics of neurodegenerative diseases.

Main text

Biological phenomena are complex dynamic events, and we need noninvasive method (without distortion of original biological structures) to monitor the dynamics to investigate mechanisms. Here, we utilize nanoplasmonic optical imaging as the noninvasive and label-free method in order to real-time monitor *in-vitro* amyloid fibrogenesis, which is considered as the primary pathological mechanism of Alzheimer's disease.

Alzheimer's disease (AD) is a neurodegenerative disease, associated with loss of memory and cognitive function[1-5]. The origin of AD is believed to be associated with brain amyloid plaques, in which the major protein constituent is a polypeptide *β*-amyloid (A*β*). The A*β* induces slow and progressive molecular structural changes, and then undergoes spontaneous growth (fibrogenesis), which causes massive plaque formation in AD patients[5, 6]. These are believed to ultimately disrupt membrane function and degenerate brain neurons, which link to cellular dysfunction and death[7-11] (Fig.1A).

Therefore it is critical to understand the kinetics of fibroogenesis of A*β* proteins to find possible theranostic solutions for AD. A few imaging techniques have been utilized such as Atomic Force Microscopy (AFM)[12-14], Transmission Electron Microscopy (TEM), fluorescent imaging with quantum dots, and optical trapping[15-21]. While these current methods have an advantage of high resolution imaging, limiting factors include invasiveness in AFM and TEM that required real-time monitoring of A*β* aggregation, photo bleaching and low quantum efficiency in fluorescent microscopy, and cellular toxicity issues in QD-based fluorescent microscopy for long-term monitoring of A*β* fibrogenesis kinetics.

In this communication, we utilize nanoplasmonic optical imaging as the noninvasive and label-free method and demonstrate as an effective real-time monitoring method of amyloid fibrogenesis using gold nanoplasmonic particles (GNPs) since the Rayleigh

scattering of GNPs has an enhanced scattering optical cross section and selective surface plasmon resonance from a specific geometry of GNP. We demonstrate this nanoplasmonic optical method to 1) compare severe and mild growth of Aβ42 in water and dimethyl sulfoxide (DMSO), respectively and 2) monitor long-term gradual self-growth of Aβ42 from mild fibril formation. For the direct observation of amyloid fibrogenesis, we dispersed GNPs in solution of Aβ peptides and tracked the Brownian movements of GNPs, which reflect degree of amyloid fibrogenesis. Using a high intensity light source from resonant Rayleigh scattering of GNPs (80 nm), which has efficiency equivalent to that of 10^6 fluorophores (*e.g.* fluorescein) [22], we accomplish efficient tracking the random movements of GNPs in Aβ solution.

This direct observation of amyloid fibrogenesis by the resonant Rayleigh scattering of GNP provides several advantages in the systematic characterization to understand the mechanism and kinetics of fibril formation and growth. Firstly, it is a non-invasive method that does not require additional sample preparation step, which cannot be avoided in TEM and AFM experiment. Secondly, label-free GNPs are very suitable to monitor long-term process since they do not have problems of photo bleaching like for fluorescent probes or blinking for quantum dot sensors. Thirdly, it can provide quantitative information of Aβ growth. The movement of single GNPs Aβ in solution can be quantified by Mean Square Displacement (MSD), which offers the information of diffusivity and elasticity during Aβ growth. The current *in-vitro* demonstration can be extended to *in-vivo* studies by utilizing NIR-optics since probes are biologically inert and easy to introduce into cells [23-26].

The localized surface plasmon resonance of GNPs (80 nm, BBI international) generates a sufficient intensity of light *via* dark-field imaging setup (Fig.1B, Fig.S1A and S1B). The bright GNPs randomly move in solution by Brownian force. We utilized these movements of GNPs to characterize the kinetics of amyloid fibril formation and growth. As

schematically shown in Fig.1C, the movement of GNP would be restricted by the amyloid fibril near the particle. As a result, we observed the movement of GNPs within/out Aβ42 (Amyloid-β42 peptide, Sigma-Aldrich). GNPs suspended in water without Aβ42 can move unrestrictedly and show broadly spread trajectories (Fig.1D). In contrast, GNPs suspended within Aβ42 solution, show a narrower trajectory, which can be interpreted as the restricted movement of GNPs by Aβ42 fibril (Fig.1C and 1D).

We took sequential images of GNPs' Rayleigh scattering in sample solution every 60 ms for 200 frames. We analyzed the single GNP's movement by mean square displacement (MSD) and its trend in accordance with observed lag time from the first analyzed time-point in the analysis of trajectory (Supplementary Text S1, Fig.S1C and S1D). The *MSD* of a particle in 2-dimensions is known as equation 1 [27, 28]. The exponent α can be obtained from slope of log-log plot: *MSD* versus the observed lag time as Fig. 2A.

$$MSD = 4D\tau^{\alpha} \qquad (D\text{: Diffusivity, } \tau\text{: observed lag time}) \qquad (1)$$

$$D = kT / 6\pi\eta R \qquad (2)$$

(*k*: Boltzmann constant, *T*: Temperature, η: viscosity, *R*: radius of particle)

We note that *MSD* of a particle in 3-dimensions could be considered with advanced platform (e.g. multi-plane imaging[29], bifocal imaging[30]) and in that case, the equation 1 would be replaced by [$MSD = 6D\tau^{\alpha}$].

Compared to conventional fluorescent particle tracking method, the nanoparticles have a benefit to increase tracking resolution in their mean square displacement (MSD). According to Einstein correlation (equation 2: $D = kT / 6\pi\eta R$), the diffusivity is inversely proportional to size of particle, and smaller particle moves further and could be more sensitive. The 80 nm GNPs used in this study can increase 12.5 (=1000 / 80) times of

sensitivity (diffusivity) in comparison to typical size (1000 nm = 1 μm) of fluorescent particle for tracking. With conventional methods, it is difficult due to limited optical resolution to visualize the submicron size of fluorescent particles without specialized costly instruments: high-resolution objective lens and highly sensitive camera (e.g. EM CCD, sCMOS camera). In contrast, the plasmonic particles (e.g. gold, silver) even in nanometer scales can be efficiently visualized by Rayleigh scattering with commonly used cameras.

In order to confirm accuracy of our nanoplasmonic particle tracking, we firstly measured the viscosity of a known polymer (Dextran; M.W.=70,000, Sigma Aldrich) solution at various concentrations, and compared to conventional viscometer (rheometer) measurements. In our particle tracking method, viscosities could be calculated from *MSD*- *τ* plots and equation 1, 2. Indeed, with increasing concentration of Dextran, the viscosity increases accordingly and the values are identical to the ones measured by conventional method (Supplementary Table S1).

Further, we characterized the effect of Aβ monomer concentration. We obtained the MSD values of GNPs at various concentrations of A*β* in water. The MSD values of GNPs without Aβ42 (plot of 0 μM in Fig.2A) are approximately 100 times larger than values of GNPs at 25 μM within a whole range of lag time (Fig.2A). As the concentration of A*β*42 peptide in water increased, the MSD values decrease accordingly (Fig.2A).

Next, we applied this approach to distinguish severe and mild fibrogenesis of A*β*42. In water A*β*42 is known to form severe fibrils, while in DMSO[31] mild fibrils form. The DMSO is a strong organic solvent and is commonly used to solubilize hydrophobic peptides such as A*β*. It also makes delay of forming A*β* fibril/aggregation. Indeed, we distinguished the severe and mild fibrogenesis of A*β*42 in water and DMSO, respectively. In the *MSD* plot and diffusivity calculated from equation 1 and 2, we observe that the effect of concentration of A*β* monomer is weaker in DMSO. With increasing concentrations of A*β*42, the MSD

values decrease in both DMSO and water (Fig.2A and 2B). Similarly, exponent α and diffusivity decrease significantly with increasing concentration (Fig.2C and 2D). Also, the exponent α decrease more evidently in water compared to DMSO (Fig.2C). Generally, the exponent α distinguishes a type of diffusion that particles encountered: α=1; normal Brownian diffusion in purely viscous (liquid-like) material *e.g*. water, α<1; sub-diffusion in elastic material, and α>1; super-diffusion or active movement. In the case of DMSO, the value is quite stable around 1 even in high Aβ42 concentration (25 μM), which indicates that Aβ42 does not severely form fibrils but maintains as viscous condition (Fig.2C). In contrast the exponent α rapidly decreased with increase of Aβ42 concentration in water. Taken together, our results confirm that Aβ42 forms more severe fibrogenesis in water and we expect this approach could be a useful new quantification method to monitor the degree of Aβ42 fibrogenesis. The exponent α would be one simple parameter for quantification, and would have an advantage over AFM analysis, in which it is not easy to quantitatively compare the degree of fibrogenesis. Additionally, we note that water and DMSO are chosen to evaluate whether our method can distinguish severe and mild fibrogenesis as a benchmark outside of the physiological condition.

Finally, we monitored the long-term kinetics of Aβ42 fibrogenesis. GNP was dispersed in Aβ42 / DMSO solution. We chose 5 μM of Aβ42 concentration as a precursor that does not severely form fibril at the beginning of incubation (Fig.2B, C and D). The MSD values, diffusivity and exponent α slowly decrease as the incubation time progressed (Fig.3A and 3B). The result is consistent with AFM studies that show fibrils slowly grow with the same experimental condition of incubation time[31]. Thus, we confirmed our nanoplasmonic optical method is relevant to characterize slow and long-term kinetics of Aβ42 fibrogenesis as well. In order to further validate the use of nanoparticle tracking to infer Amyloid Beta peptide aggregation and understand essential mechanistic details of Aβ

fibrogenesis, it would be ideal to combine with current existing technologies such as AFM, NMR, DLS and numerical simulation[35, 36] that provide morphological and structural information of A*β*.

In summary, we presented a noninvasive and label-free method by utilizing nanoplasmonic optical imaging that efficiently tracks and quantifies random movements of GNPs' by resonant Rayleigh scattering and demonstrated an effective real-time characterization method of Aβ fibrogenesis. We expect this approach could be utilized to research in neurodegenerative disease such as Alzheimer's disease (AD) pharmacology for developing an innovative strategy to delay or prevent the onset of amyloid growth and elucidating *in-vivo* mechanism of amyloid growth in AD. GNPs have a lot of potential since 1) they are biologically inert and easy to introduce into the living neuronal cells and the darkfield imaging is already demonstrated in *in-vivo* imaging[32, 33], 2) they are easy to functionalize surface for specific detection and delivery of key biomolecules, and 3) they can be used as nanoplasmonic optical antennas in living cells for both gene delivery and monitoring toward the theranostics of neurodegenerative diseases[26, 34], although we need to consider potential cause to affect on the GNP movement *in-vivo* system such as intracellular organelles. In addition, the systematic studies of interaction effect between GNP and A*β* should be carried out for more accurate quantification of kinetics in fibrogenesis since methionine in A*β* sequence would form Au-S bonding with GNP.

Moreover, this non-invasive label-free nanoplasmonic particle tracking method would be utilized as precision biophysical measurements in quantitative cell biology. Many cellular and subcellular processes depend critically on the mechanical deformability of the cytoplasm. For example, the translocation of organelles (e.g., nucleus, endoplasmic reticulum and mitochondria) within the cytoplasm is partly associated with local viscoelastic (physical) properties of the cytoplasm. GNPs would be introduced directly into the

cytoplasm of live cells and we would probe the viscoelastic properties of various types of cells in a wide range of conditions. These measurements would provide us invaluable insight how the biophysical properties of the cytoplasm cope with various chemical and physical stimuli, how they can regulate basic cell functions, and how these properties can be significantly altered in diseased cells together. Additionally, these GNPs would have functionalized surfaces so that they would be utilized as physico/chemo multi-probes that measure mechanical (viscoelastic) properties and detect specific key molecules.

Acknowledgements

The authors acknowledge support from ETH Zurich (D-BSSE) and Electronics and Telecommunication Research Institute (ETRI). The authors also thank H. Kang and Y. Yim for providing IDL code for particle tracking, and S. Pun for helpful discussion of experiment. We are grateful to Dr. Alicia Smith for helpful comments on this manuscript.

Additional information

Supplementary material is available in the online version of this article.

REFERENCES

1. G. G. Glenner and C. W. Wong, *Biochem Biophys Res Commun*, 1984, **120**, 885-890.

2. A. Goate, M. C. Chartierharlin, M. Mullan, J. Brown, F. Crawford, L. Fidani, L. Giuffra, A. Haynes, N. Irving, L. James, R. Mant, P. Newton, K. Rooke, P. Roques, C. Talbot, M. Pericakvance, A. Roses, R. Williamson, M. Rossor, M. Owen and J. Hardy, *Nature*, 1991, **349**, 704-706.

3. Y. M. Kuo, M. R. Emmerling, C. VigoPelfrey, T. C. Kasunic, J. B. Kirkpatrick, G. H. Murdoch, M. J. Ball and A. E. Roher, *Journal of Biological Chemistry*, 1996, **271**, 4077-4081.

4. P. T. Lansbury and H. A. Lashuel, *Nature*, 2006, **443**, 774-779.

5. R. E. Tanzi, *Nature Neuroscience*, 2005, **8**, 977-979.

6. G. Bitan, M. D. Kirkitadze, A. Lomakin, S. S. Vollers, G. B. Benedek and D. B. Teplow, *Proc Natl Acad Sci U S A*, 2003, **100**, 330-335.

7. C. J. Pike, D. Burdick, A. J. Walencewicz, C. G. Glabe and C. W. Cotman, *Journal of Neuroscience*, 1993, **13**, 1676-1687.

8. B. Seilheimer, B. Bohrmann, L. Bondolfi, F. Muller, D. Stuber and H. Dobeli, *J Struct Biol*, 1997, **119**, 59-71.

9. G. M. Shankar and D. M. Walsh, *Mol Neurodegener*, 2009, **4**, 48.

10. M. M. Stevens and J. H. George, *Science*, 2005, **310**, 1135-1138.

11. M. Bartolini, M. Naldi, J. Fiori, F. Valle, F. Biscarini, D. V. Nicolau and V. Andrisano, *Analytical Biochemistry*, 2011, **414**, 215-225.

12. L. Connelly, H. Jang, F. T. Arce, R. Capone, S. A. Kotler, S. Ramachandran, B. L. Kagan, R. Nussinov and R. Lal, *Journal of Physical Chemistry B*, 2012, **116**, 1728-1735.

13. H. Jang, F. T. Arce, S. Ramachandran, R. Capone, R. Azimova, B. L. Kagan, R. Nussinov and R. Lal, *Proc Natl Acad Sci U S A*, 2010, **107**, 6538-6543.

14. A. Quist, L. Doudevski, H. Lin, R. Azimova, D. Ng, B. Frangione, B. Kagan, J. Ghiso and R. Lal, *Proc Natl Acad Sci U S A*, 2005, **102**, 10427-10432.

15. T. P. J. Knowles, W. M. Shu, G. L. Devlin, S. Meehan, S. Auer, C. M. Dobson and M. E. Welland, *Proc Natl Acad Sci U S A*, 2007, **104**, 10016-10021.

16. Y. Kusumoto, A. Lomakin, D. B. Teplow and G. B. Benedek, *Proc Natl Acad Sci U S A*, 1998, **95**, 12277-12282.

17. R. Liu, H. Barkhordarian, S. Emadi, C. B. Park and M. R. Sierks, *Neurobiol Dis*, 2005, **20**, 74-81.

18. M. R. Nilsson, *Methods*, 2004, **34**, 151-160.

19. T. Witte, L. A. Haller, E. Luttmann, J. Kruger, G. Fels and K. Huber, *J Struct Biol*, 2007, **159**, 71-81.

20. A. J. Veloso, H. Yoshikawa, X. R. Cheng, E. Tamiya and K. Kerman, *Analyst*, 2011, **136**, 4164-4167.

21. K. Tokuraku, M. Marquardt and T. Ikezu, *PLoS One*, 2009, **4**, e8492.

22. J. Yguerabide and E. E. Yguerabide, *Analytical Biochemistry*, 1998, **262**, 137-156.

23. K. Aslan, J. R. Lakowicz and C. D. Geddes, *Current Opinion in Chemical Biology*, 2005, **9**, 538-544.

24. I. H. El-Sayed, X. H. Huang and M. A. El-Sayed, *Nano Letters*, 2005, **5**, 829-834.

25. P. K. Jain, K. S. Lee, I. H. El-Sayed and M. A. El-Sayed, *Journal of Physical Chemistry B*, 2006, **110**, 7238-7248.

26. S. E. Lee, G. L. Liu, F. Kim and L. P. Lee, *Nano Lett*, 2009, **9**, 562-570.

27. T. G. Mason, K. Ganesan, J. H. vanZanten, D. Wirtz and S. C. Kuo, *Physical Review Letters*, 1997, **79**, 3282-3285.

28. T. A. Waigh, *Reports on Progress in Physics*, 2005, **68**, 685-742.

29. S. Ram, E. S. Ward and R. J. Ober, *Proc Natl Acad Sci U S A*, 2006, **103**, 4457-4462.

30. E. Toprak, H. Balci, B. H. Blehm and P. R. Selvin, *Nano Letters*, 2007, **7**, 2043-2045.

31. W. B. Stine, K. N. Dahlgren, G. A. Krafft and M. J. LaDu, *Journal of Biological Chemistry*, 2003, **278**, 11612-11622.

32. Y. H. Choi, T. Kang and L. P. Lee, *Nano Letters*, 2009, **9**, 85-90.

33. X. H. Huang, I. H. El-Sayed, W. Qian and M. A. El-Sayed, *Journal of the American Chemical Society*, 2006, **128**, 2115-2120.

34. G. L. Liu, Y. T. Long, Y. Choi, T. Kang and L. P. Lee, *Nature Methods*, 2007, **4**, 1015-1017.

35. B. Y. Ma and R. Nussinov, *Current Opinion in Chemical Biology*, 2006, **10**, 445-452.

36. J. E. Gillam and C. E. MacPhee, *Journal of Physics-Condensed Matter*, 2013, **25**, 373101

FIGURES

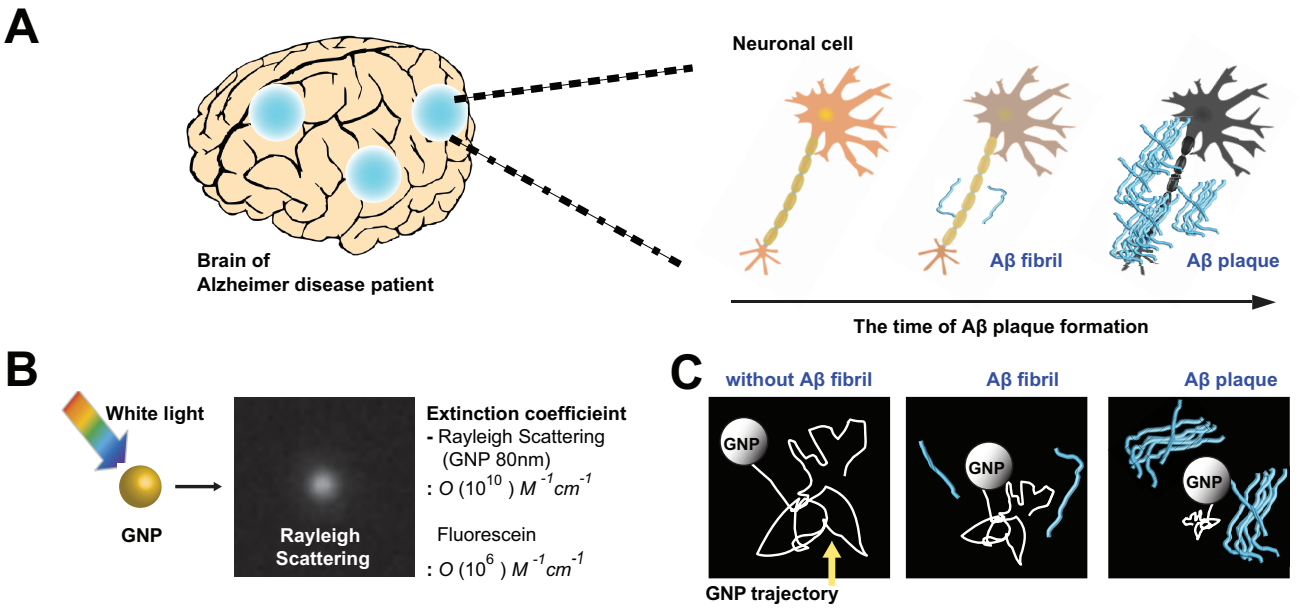

Figure 1

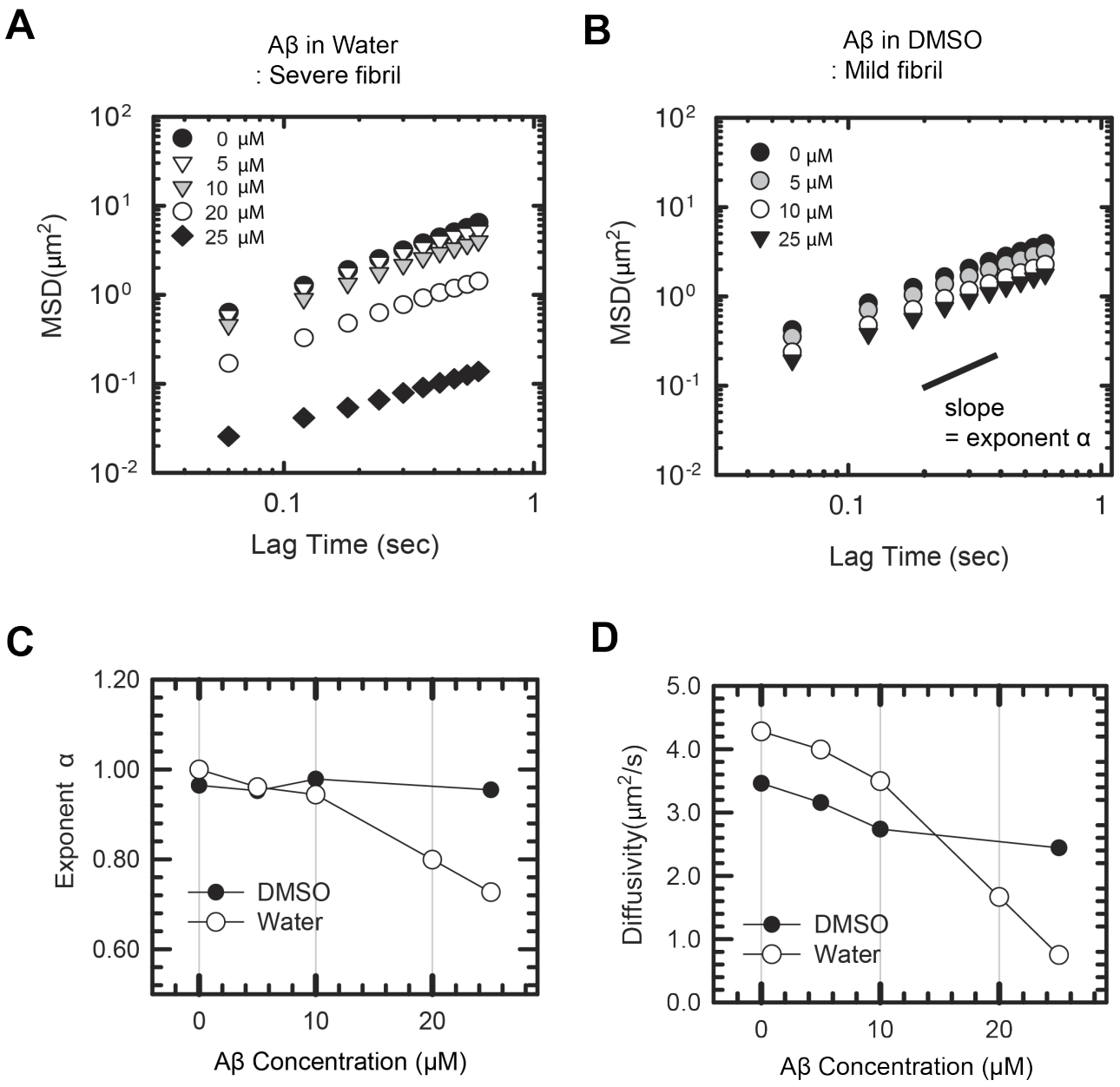

Figure 2

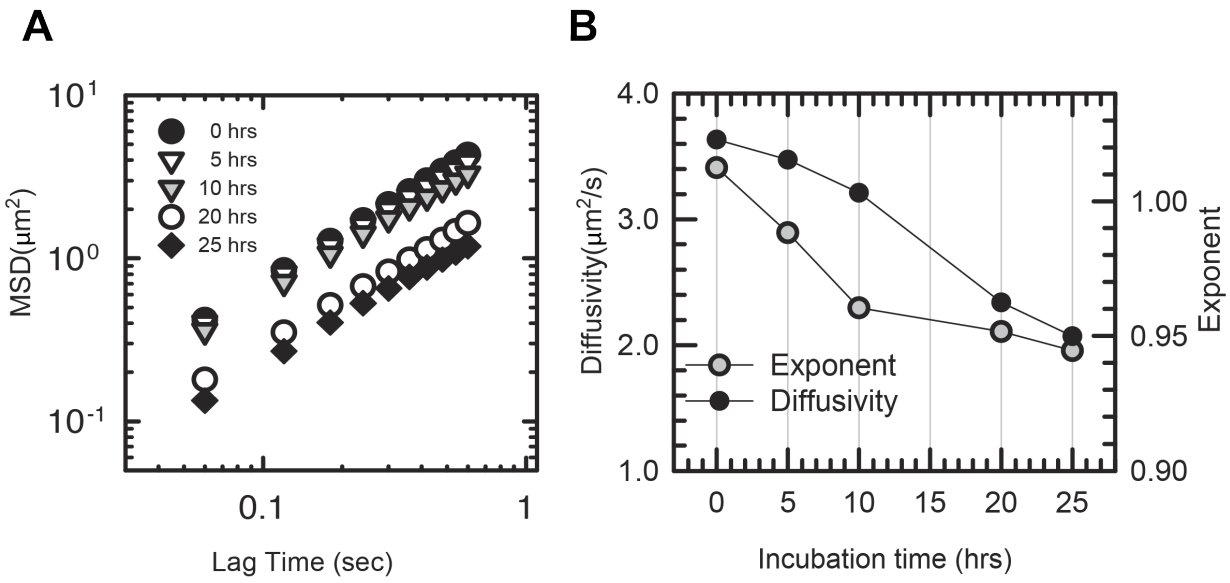

Figure 3

FIGURE CAPTIONS

Figure 1. Amyloid β42 (A*β*42) plaque formation in Alzheimer disease patient (AD), and real-time monitoring of the amyloid fibrogenesis by noninvasive label-free nanoplasmonic optical imaging, which allows quantitative analysis: (A) In the brain of Alzheimer's disease patient (AD), the neuronal plaques are found, which is aggregation of insoluble amyloid β (Aβ) peptides. It is believed to make the death of neuronal cells and cause loss of memory and cognitive function. The A*β* slowly undergoes spontaneous growth (fibrogenesis), and massively forms plaques. **(B)** Rayleigh scattering of single gold nanoplasmonic particle (GNP): It can be visualized by dark-field imaging by combination of condenser and objective lens (numerical aperture (N.A.) of condenser is higher than one of objective lens). The efficiency of the GNP scattering (extinction coefficient) is equivalent to that of 10^6 fluorophores (e.g. fluorescein) so that it is easy to visualize the single nanoplasmonic probe. **(C)** Schematic illustration of GNP trajectory that reflect the process of amyloid fibrogensis without amyloid fibril in initial state (left), mild amyloid fibril (middle) and severe amyloid plaque (right). **(D)** The movement of GNPs are restricted by amyloid. Typical trajectories of GNPs dispersed in water without A*β*42 (left) and with 25 *μ*M of A*β*42 (right). The movement of GNPs' Rayleigh scattering was tracked with images taken by every 60 ms.

Figure 2. Noninvasive label-free nanoplasmonic optical method, which allows direct monitoring of the effect of Amyloid β42 (A*β*42) concentration and dispersed medium that form severe and mild fibril (A) Severe amyloid fibril: Mean square displacement (MSD) in water **(B)** Mild amyloid fibril: Mean square displacement (MSD) in DMSO **(C)**

Diffusivity and **(D)** exponent obtained from correlation between MSD and lag time: $MSD = 4D\tau^{\alpha}$ (D: Diffusivity, α: Exponent), α is the slope of MSD versus lag time in **(A)** and **(B)**.

Figure 3. Long-term real-time monitoring of progressive amyloid β42 (A*β*42) fibrogenesis by noninvasive label-free nanoplasmonic optical method Amyloid β42 (Aβ42) is incubated in DMSO. **(A)** Mean square displacement (MSD) **(B)** Diffusivity and exponent obtained from correlation between MSD and lag time: MSD = $4D\tau^{\alpha}$ (D: Diffusivity, α: Exponent).

TOC Figure

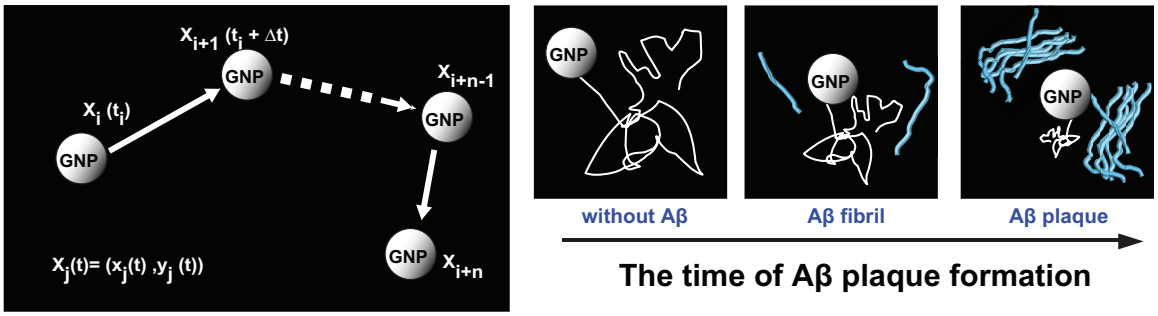

We utilize nanoplasmonic optical imaging as the noninvasive and label-free method in order to monitor *in-vitro* amyloid fibrogenesis in real-time, which is considered as the primary pathological mechanism of Alzheimer's disease.